PHYSICAL REVIEW B VOLUME 28, NUMBER 12 15 DECEMBER 1983

Electronic structure of ion-implanted graphite

B. S. Elman
Department of Physics and Center for Materials Science and Engineering, Massachusetts Institute of Technology, Cambridge, Massachusetts 02139

L. McNeil and C. Nicolini*
Center for Materials Science and Engineering, Massachusetts Institute of Technology, Cambridge, Massachusetts 02139

T. C. Chieu† and M. S. Dresselhaus
Department of Electrical Engineering and Computer Science and Center for Materials Science and Engineering, Massachusetts Institute of Technology, Cambridge, Massachusetts 02139

G. Dresselhaus
Francis Bitter National Magnet Laboratory, Massachusetts Institute of Technology, Cambridge, Massachusetts 02139
(Received 8 August 1983)

The magnetoreflection technique is applied to study Landau-level transitions in graphite implanted with ^{31}P ions at a variety of fluences and energies. The magnetoreflection spectra are explained in terms of the Slonczewski-Weiss-McClure band model with small changes in the band parameters that describe pristine graphite. Neglecting trigonal warping, the fluence dependence of the nearest-neighbor intraplanar (γ_0) and interplanar (γ_1) overlap integrals is presented. The observed changes in these band parameters are consistent with increasing disorder as the fluence of implantation increases.

INTRODUCTION

Ion implantation provides a physical mechanism for the introduction of foreign species into semiconductors[1] (e.g., Si, Ge, GaAs, etc.) and semimetals[2–6] (e.g., graphite and bismuth). One of the advantages of the implantation method is that it makes possible the introduction of foreign species that for various reasons cannot be introduced chemically into the host material.

A number of major changes occur in the host material during the ion-implantation process. Firstly, radiation damage to the crystalline host is produced. Atoms of the parent material are displaced from their lattice sites by cascade processes caused by the entry of highly energetic guest ions into the host material. The effect of radiation damage to the substrate and the spatial distribution of the radiation damage has been extensively studied in both semiconductors and semimetals by a variety of techniques.[1,7–9] Radiation damage phenomena are not of interest in the present work. Another interesting feature of the ion-implantation process is the implantation-induced change in the carrier concentration of the substrate. This effect has also been extensively studied, especially for semiconductors.[1] However, the implantation-induced modification of the electronic structure of the substrate has received little attention, but is also of great interest and importance.

This paper focuses on a quantitative determination of the implantation-induced modifications of the electronic structure of the semimetal graphite, which is studied by the magnetoreflection technique. In essence, the magnetoreflection experiment measures the relative changes in the reflectivity from the surface of the sample as a function of applied magnetic field. One of the advantages of this technique in studies of ion-implanted materials is that the optical skin depth (δ) is comparable to the penetration depth of the implanted ions (R_p), so that the optical experiments are especially sensitive to the region of interest. Furthermore, magneto-optical studies provide a powerful tool for the study of the electronic structure of semimetals because of the low effective masses characteristic of this class of materials and because of the consequent ease of satisfying the conditions $\omega_c\tau > 1$ and $\hbar\omega_c > kT$, which are necessary requirements for the observation of resonant magneto-optical effects. The condition $\omega_c\tau > 1$ (where ω_c is the cyclotron angular frequency $\omega_c = eH/m_c^* c$, m_c^* is the cyclotron effective mass, and τ is the relaxation time) implies that an electron or hole completes at least one cyclotron orbit before being scattered. This clearly indicates that the experiment is also sensitive to the density of scattering centers in the volume of interest, which is directly related to the extent of the implantation-induced damage to the substrate. The condition $\hbar\omega_c > kT$ implies that the characteristic magnetic energy $\hbar\omega_c$ is large compared with thermal energies, so that distinct Landau levels can be resolved when in competition with thermal broadening effects. We should emphasize that magneto-optical studies have been carried out on semiconductors,[10,11] group-V semimetals,[12–14] and pristine graphite[15–17] and not only provide a useful tool for the determination of their electronic structures but also of the changes induced by perturbations such as variation of

pressure,[18] temperature,[19] and composition[20] (alloying and intercalation). The method has been also successfully applied to the studies of ion-implanted bismuth.[6,21]

We analyze the experimental magnetoreflection spectra from ion-implanted graphite in terms of the Slonczewski-Weiss-McClure (SWMcC) model, which is based on the crystal symmetry of the perfect crystal and gives an analytical expression for the electronic states near the Fermi energy E_F.[22,23] The model expresses the electron dispersion relations in terms of seven parameters (Δ, γ_i, $i=0,1,\ldots,5$), which in practice are determined experimentally. Some of the parameters, such as γ_0 and γ_1, the intraplanar and interplanar nearest-neighbor overlap integrals, are expected to change as a function of the implantation parameters, and this is in fact reported in the present work. The findings are consistent with long-range effects on the electronic structure of the substrate during the process of ion implantation. Similar effects have been reported for the case of ion-implanted bismuth.[6]

EXPERIMENTAL DETAILS

Magnetoreflection data have been taken on c faces of pristine and ion-implanted highly oriented pyrolytic graphite (HOPG) samples.[24] Sample preparation and characterization techniques are described below.

To achieve the resonant condition $\omega_c\tau \gg 1$, the HOPG samples were implanted at elevated temperatures (implantation temperature $T_i \sim 600\,^\circ$C). The sample holder for high-temperature implantation is described elsewhere,[5] as is the effect of mechanical damage to the HOPG surface when the implantation is carried out at room temperature.[4] Elevated temperatures of implantation were used to reduce lattice damage in the region where the implanted ions pass and stop, and to reduce the mechanical damage to the HOPG surface. Ions of ^{31}P were implanted at a variety of fluences ϕ and energies E in the range $8.5\times10^{13} < \phi < 1.0\times10^{15}$ ions/cm^2 and $70 < E < 200$ keV. The penetration depth (R_p) and the corresponding Gaussian halfwidth of the implanted ions (ΔR_p) in HOPG for this range of ion energies are in the range $670 < R_p < 1980$ Å and $220 < \Delta R_p < 470$ Å when the implantation is done at room temperature.[25]

At elevated temperatures of ion implantation (e.g., $T_i \simeq 600\,^\circ$C), we demonstrated using the secondary-ion mass spectroscopy (SIMS) technique[5] that because of the special properties of the HOPG material, no enhanced diffusion of foreign species across the planes was observed. Therefore the distribution and concentration of ions implanted into the hot samples of HOPG is nearly the same for $30\,^\circ\text{C} < T_i \leq 800\,^\circ$C as after the room-temperature implantation.

Before the magnetoreflection experiments were done, the ion-implanted samples were characterized with Raman spectroscopy. As previously reported,[3,4] Raman spectra are sensitive to the amount of implantation-induced disorder in HOPG. Furthermore, the in-plane microcrystallite size within the optical skin depth is easily determined from the ratio of intensities of the disorder-induced (I_{1360}) line to the Raman-allowed (I_{1580}) line in the first-order spectra.[26] A typical first-order Raman spectrum from one of the samples studied in the present magnetoreflection experiments is shown in Fig. 1. For this particular sample, the value of $R = I_{1580}/I_{1360}$ is about 12, which corresponds to an in-plane crystallite size $L_a \sim 400$ Å.[26] By studying the Raman spectra for a variety of different samples, we found that reasonably sharp transitions in the magnetoreflection spectra with fairly good signal-to-noise ratios were observed when the ratio R exceeds 8 and the penetration depth of implanted ions R_p is less than 2000 Å.

The magnetoreflection measurements were made in the Faraday geometry at low temperatures (using a cold-finger Dewar cooled by liquid helium) and at high magnetic fields up to 15 T to satisfy the conditions $\omega_c\tau \gg 1$ and $\hbar\omega_c > kT$. The reflecting area of the samples was about 12×8 mm^2 and the sample thickness about 1.5 mm. Infrared radiation was provided by a globar. Particular photon energies in the range $99 \leq \hbar\omega \leq 300$ meV were chosen with a single-pass monochromator. Because the selection rules for the observed transitions depend on the sense of circular polarization, the data were taken with positively and negatively circularly polarized light. The reflected light was detected by a cooled (liquid-helium) Cu-Ge photodetector. The sample geometry is shown in Fig. 2. The experimental arrangement for the magnetoreflection experiment is discussed elsewhere.[11]

Zero magnetic field infrared spectra (Fig. 3) on the same set of samples were taken on a Fourier-transform spectrometer in the reflection geometry. The experimental conditions of the ir experiment are described elsewhere,[27] as is the analysis of the ir reflectivity spectra of graphite to yield information on the free-carrier contribution to the dielectric function.[27]

RESULTS AND ANALYSIS

The magnetoreflection technique permits a direct determination of the change in electronic structure associated with the ion-implantation process. In this analysis we use

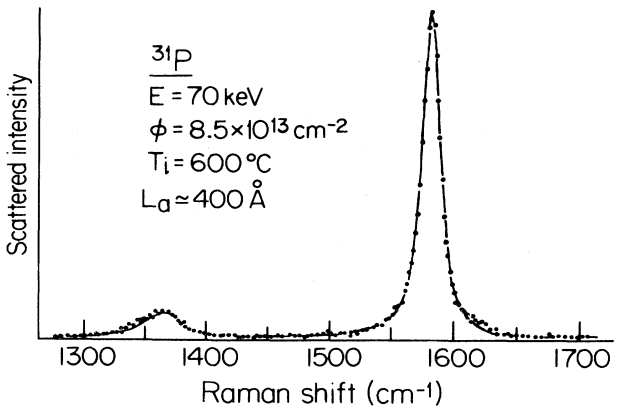

FIG. 1. First-order Raman spectrum of HOPG ion implanted with ^{31}P ($E=70$ keV) at a fluence $\phi = 8.5\times10^{13}$ ions/cm^2. The temperature of the sample during implantation was $T_i = 600\,^\circ$C. The abscissa is linear in wave number and the points are experimental. The solid curve is a Lorentzian fit to the points. For this sample $R = I_{1580}/I_{1360} \sim 12$.

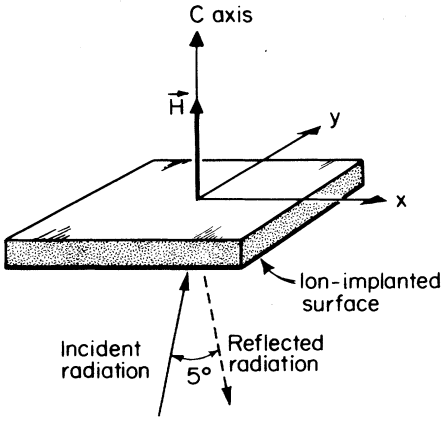

FIG. 2. Sample geometry of the magnetoreflection experiment.

the spectra for unimplanted graphite as a reference and present the changes in electronic structure near the Fermi level in terms of changes in the band parameters of graphite as given by the well-established Slonczewski-Weiss-McClure (SWMcC) band model.[22,23] This model is based on the crystal symmetry of graphite and gives an analytic expression for the electronic states $E(\vec{k})$ near the $H-K$ axis of the Brillouin zone. For the case of graphite, Landau-level transitions are observed for both the H and K points in the Brillouin zone, and the H- and K-point transitions each yield complementary information about the electronic structure.[15–18]

To illustrate how the H- and K-point transitions are identified in the magnetoreflection spectra, we refer to Fig. 4 of Ref. 17. In the present study, magnetoreflection

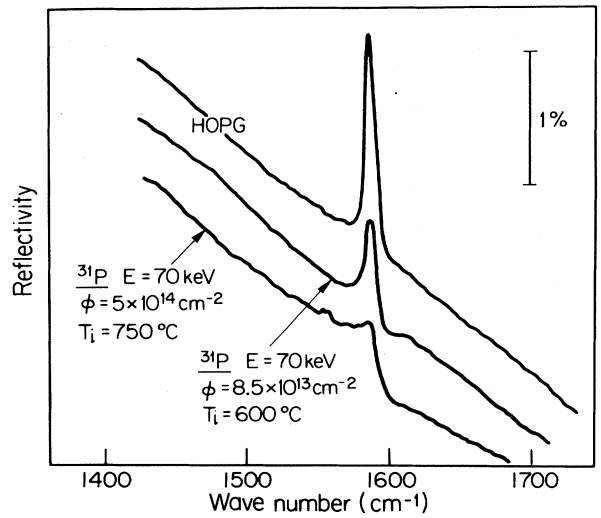

FIG. 3. Room-temperature c-face reflectivity spectra of the infrared-active phonons for the energy range $1400<\omega<1800$ cm^{-1} for unimplanted pristine graphite and for two of the ion-implanted HOPG samples. The fluence ϕ and energy E for the ^{31}P ions are given for the samples implanted at temperature T_i.

spectra similar to those in Refs. 15–18 were obtained for unimplanted HOPG and for HOPG implanted with ^{31}P ions at 70 keV and three different ion fluences using a hot-stage sample holder at implantation temperature T_i. We show in Figs. 4(a) and 4(b) typical spectra for these samples for positive and negative circular polarization, respectively. In each spectrum the corresponding Landau-level transitions for the K-point transitions are labeled by the quantum numbers n_i and n_f for the initial and final states, respectively, using the notation (n_i,n_f).

The analysis of the H-point spectra follows the work of Toy *et al.*[17] The transition energies at the H point are given by

$$\hbar\omega_m^{(+)}=\hbar\omega_m^{(-)}=\tfrac{1}{2}(\Delta^2+4NB)^{1/2}+\tfrac{1}{2}[\Delta^2+4(N+1)B]^{1/2}\,, \quad N\geq 1 \qquad (1)$$

where $B=3\gamma_0^2 a_0^2 eH/2\hbar c$, and H is the applied magnetic field, a_0 is the graphite lattice spacing, and the H-point transitions are labeled by $m=N$ corresponding to $N\rightarrow N+1$ and $N+1\rightarrow N$ transitions. Since these energies depend sensitively on γ_0, the nearest-neighbor intraplanar overlap integral, analysis of the H-point spectra provides direct information on the implantation-induced expansion of the in-plane honeycomb lattice. Because of the extremely strong in-plane bonding in graphite, it is expected that this expansion will be very small. Nevertheless, these changes are sufficiently large to be observable in the H-point magnetoreflection spectra. Figure 5 shows results for the $m=1$ H-point transitions observed over a wide range of photon energies in unimplanted graphite (open circles) and for the same ion-implanted graphite samples as in Fig. 4. With the use of Eq. (1), a fit to the H-point spectra was made for both the unimplanted and implanted samples. For the unimplanted HOPG spectra, good agreement was obtained between our H-point spectra and those of Toy *et al.*[17] Since the parameter Δ is very small, the spectra depend almost entirely on the value of γ_0. Thus for all samples in Fig. 5 the value for Δ was fixed at $\Delta=-0.008$ eV, the value previously determined for the unimplanted sample.[17] The parameter γ_0 was then determined by a fit to the H-point spectra for each of the implanted samples. Reproducible data for the implanted samples were limited to the $m=1$ H-point transition (see Fig. 5). The results obtained for the relative changes in γ_0 for the ^{31}P-ion-implanted samples $\gamma_0^{\rm imp}$ with respect to γ_0 for pristine unimplanted HOPG ($\gamma_0^{\rm HOPG}=3.11$ eV) versus the ion fluence (log scale) are given by the solid circles in Fig. 6. Unfortunately, the data are not sufficiently extensive to distinguish reliably between different possible functional dependences of $(\gamma_0^{\rm imp}/\gamma_0^{\rm HOPG})$ on fluence ϕ. We must emphasize at this point that we were not able to determine these data over a much expanded range of fluence, keeping other parameters of implantation the same. Our sensitivity is not sufficient to detect changes in γ_0 for $\phi<10^{13}$ cm^{-2}. Furthermore, at $\phi>10^{15}$ cm^{-2}, the spectra become too broad and weak to permit quantitative analysis of the H-point spectra. The decrease of γ_0 with increasing ϕ in Fig. 6 is consistent with an expansion of the in-plane structure due to the strain produced by the additional ions resident in the implanted region between

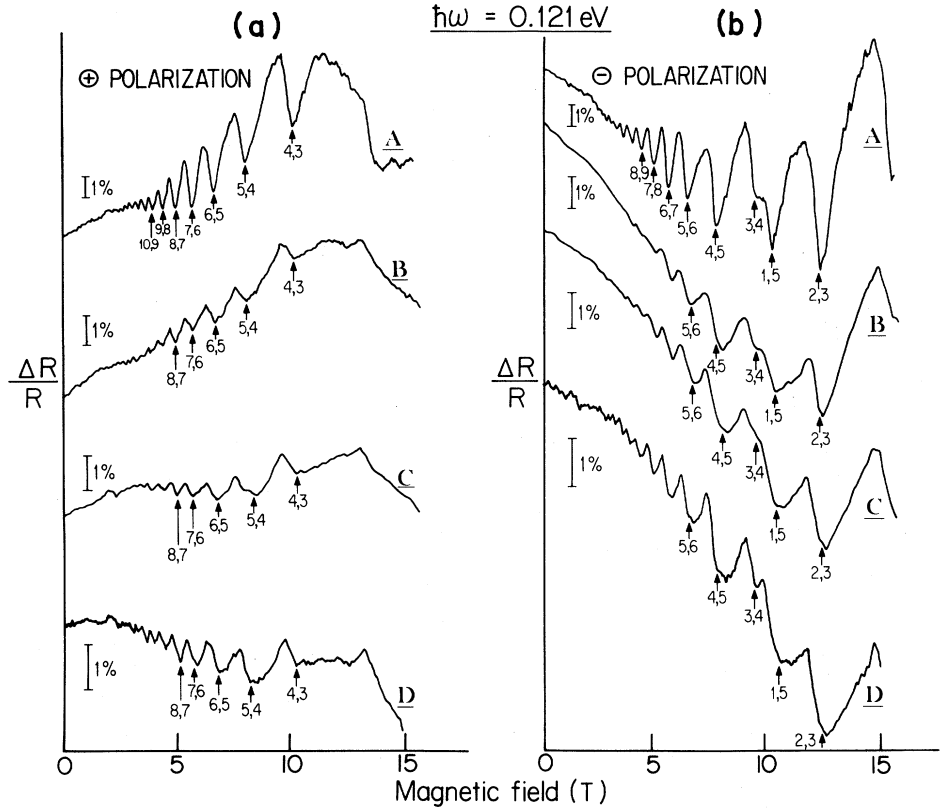

FIG. 4. Magnetoreflection traces for (a) positively polarized and (b) negatively polarized light taken on pristine HOPG and on HOPG ion implanted with ^{31}P ions ($E=70$ keV) at different fluences and temperatures of implantation. *A*, unimplanted pristine HOPG; *B*, $\phi=8.5\times10^{13}$ cm^{-2}, $T_i=600$ °C; *C*, $\phi=5.0\times10^{14}$ cm^{-2}, $T_i=750$ °C; and *D*, $\phi=1.0\times10^{15}$ cm^{-2}, $T_i=600$ °C. For all the traces, the photon energy is $\hbar\omega=0.121$ eV. The *K*-point transitions are labeled by their initial, final levels.

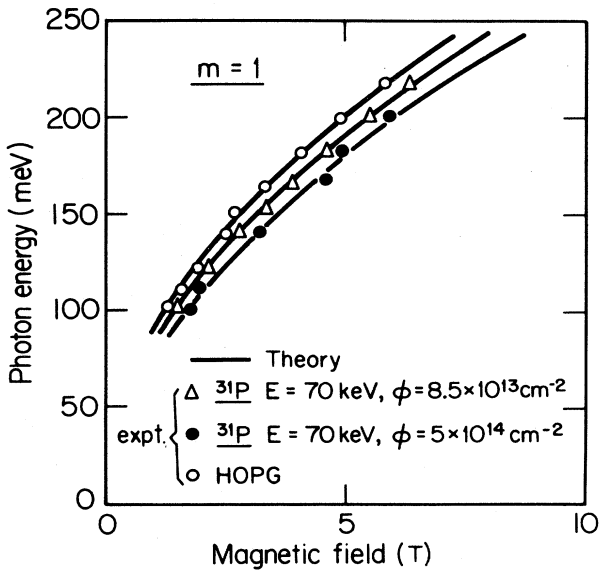

FIG. 5. Summary of the $m=1$ *H*-point resonances covering a wide range of photon energies and magnetic fields. The curves passing through the experimental points represent a least-squares fit of these data to Eq. (1).

$R_p-\Delta R_p$ and $R_p+\Delta R_p$.

Information on the interplanar interactions is provided by the *K*-point transitions which are the strong, closely-spaced resonances that dominate the magnetoreflection spectra in Figs. 4(a) and 4(b). The spectra for unimplanted graphite have been extensively studied and values for the pertinent band parameters have been established.[16,17,28]

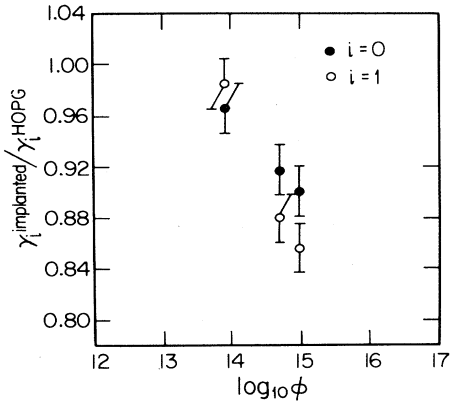

FIG. 6. Values for the γ_0 and γ_1 parameters for implanted samples with respect to those for pristine unimplanted HOPG vs fluence ϕ of ^{31}P ions implanted at energy $E=70$ keV and $T_i\sim600$ °C. Note the log scale for ϕ.

The K-point transitions are most sensitive to the parameter combination γ_0^2/γ_1, which determines the slopes for each of the K-point transitions on the fan chart for K-point transitions discussed below. The difference in resonant magnetic fields between the transitions for positive and negative polarizations is sensitive to γ_4, which is related to a difference in effective mass between the valence and conduction bands.

For the case of unimplanted graphite, the band parameters are found by analysis using the full Slonczewski-Weiss-McClure Hamiltonian.[15] The spectra in Fig. 4 show that implantation significantly broadens the K-point spectra and decreases the intensity of the resonances. Since the implantation-induced shifts in the resonant magnetic field of the dominant Landau-level transitions are small, it is possible to make tentative assignments of the Landau-level transitions for ion-implanted graphite by comparison with the spectrum for pristine graphite at the same photon energy. With the use of these assignments, it is convenient to analyze our results in terms of a simple two-band model to determine the small implantation-induced changes in band parameters. A similar analysis was previously applied successfully to interpret the small pressure-induced changes in the graphite band parameters.[18]

In the simple two-band model only two bands are considered to be strongly coupled, and coupling to all other bands is ignored. The bands at the K point are presumed parabolic in shape and the energies at the magnetic subband extrema are given by

$$E_v(N_v)=E_3^0-(N_v+\tfrac{1}{2})\hbar\omega_v^* , \tag{2}$$

$$E_c(N_c)=E_3^0+(N_c+\tfrac{1}{2})\hbar\omega_c^* , \tag{3}$$

where E_3^0 is the K-point band-edge energy, N_v and N_c label the valence- and conduction-band Landau levels, and the cyclotron frequencies ω_v^* and ω_c^* for the valence and conduction bands are defined as

$$\omega_v^*\equiv\frac{eH}{m_v^*c},\quad \omega_c^*\equiv\frac{eH}{m_c^*c} , \tag{4}$$

where m_v^* and m_c^* are the cyclotron effective masses for the valence and conduction bands with $\vec{H}\|c$ axis. For the analysis, it is convenient to introduce the mass parameters m^* and λ defined by

$$\frac{1}{m^*}=\frac{1}{2}\left[\frac{1}{m_v^*}+\frac{1}{m_c^*}\right] , \tag{5}$$

$$\lambda=\left[\frac{1}{m_c^*}-\frac{1}{m_v^*}\right]\Big/\left[\frac{1}{m_v^*}+\frac{1}{m_c^*}\right] . \tag{6}$$

These mass parameters can be related to the band parameters of the SWMcC model by[18]

$$\frac{1}{m^*}=\frac{3}{4}\frac{a_0^2}{\hbar^2}\frac{\gamma_0^2}{\gamma_1} \tag{7}$$

and

$$\lambda=\frac{4\gamma_4}{\gamma_0}-\frac{2\gamma_2-2\gamma_5-\Delta}{2\gamma_1} , \tag{8}$$

where a_0 is the in-plane graphite lattice spacing. By combining Eqs. (2)—(6) with the selection rule $N_c-N_v=\mp1$ and defining $N\equiv N_v+N_c$, we obtain for the resonant condition

$$E_c-E_v=\hbar\omega=(N+1\mp\lambda)\frac{e\hbar}{m^*c}H_N^{\pm} , \tag{9}$$

where ω is the photon frequency and the upper (lower) sign refers to positive (negative) circular polarization, and $H_N^{\pm}$ labels the resonant magnetic field corresponding to N.

It is clear from Eq. (9) that at a given photon energy the resonant magnetic field is approximately inversely proportional to the quantum number N. As indicated below, it is this relation which is used to confirm the quantum-number assignments given in Fig. 4 to the Landau-level transitions for the implanted samples.

Figure 7 represents a plot of the inverse resonant magnetic field as a function of $N+1$ for four different photon energies with negative polarization. The results for both the unimplanted and one of the implanted samples show the expected periodicity in $1/H$ [Eq. (9)], thus confirming the validity of the selection rule $\Delta N=\pm1$ and providing the quantum number assignment for the K series in the magnetoreflection spectra for the implanted sample of Fig. 7. A similar analysis was made for all the implanted samples to establish the quantum number assignments.

We should emphasize that the slopes of the lines in Fig. 7 are inversely proportional to m^*, which implies that m^* increases as a result of implantation. On the basis of a detailed analysis of the results in Fig. 7, we found that implantation of ^{31}P ions at 70 keV increases the effective mass by approximately 6% with a very small dependence on fluence for the fluence range of these experiments. From Eq. (7), knowledge of m^* yields the band-parameter combination γ_0^2/γ_1. Combining this result with the value for γ_0 obtained from the H-point transitions, we are able to determine values for γ_1, and these are shown in Fig. 6 for three fluences of ^{31}P implanted into HOPG at 70 keV and at elevated temperatures.

Although the errors are large, the results of Fig. 6 show that γ_1 decreases upon implantation, with greater de-

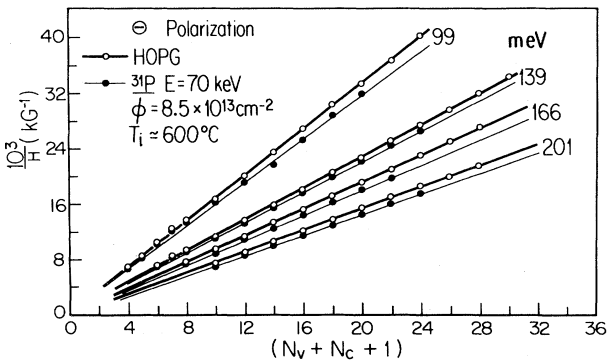

FIG. 7. Inverse resonant magnetic field as a function of the quantum number $(N+1)$ at four different photon energies and negatively polarized radiation. For comparison we show the data for pristine HOPG and for HOPG ion implanted with ^{31}P ($E=70$ keV) at $\phi=8.5\times10^{13}$ cm^{-2} ($T_i\sim600$ °C).

creases in γ_1 occurring for higher fluences. The results further show that the decreases in γ_1 are greater than the decreases in γ_0 for a given fluence. As explained below, the sign and relative magnitudes of the decreases in γ_0 and γ_1 can be understood from simple physical arguments.

In principle it is possible to obtain values for the parameter λ, from analysis of results such as in Fig. 7, but in the present experiment, the errors in determining λ were sufficiently large to overwhelm any observable changes resulting from implantation. This is not surprising, since for unimplanted graphite the value of λ is also not well known; thus it has been difficult to determine the implantation-induced change in the value of γ_4 from such an analysis. A similar difficulty has been reported in the evaluation of the pressure-dependent changes of γ_4.[18]

An analysis of the K-point spectra for the implanted samples was also carried out using the full SWMcC model. Fan charts obtained for the pristine HOPG sample and the HOPG sample implanted with 5×10^{14} cm^{-2} ^{31}P ions at 70 keV are shown in Figs. 8(a) and 8(b) for positive and negative circular polarization. The symbols represent experimental points and the solid lines are fits to the points using the γ_0 and γ_1 values determined from the two-band model. The analysis using the full SWMcC model thus yields results consistent with those obtained from the two-band model.

The magnetoreflection spectra also provide information relevant to transport properties of the implanted materials. From the resonant linewidths of the magnetoreflection spectra, we can obtain an estimate for $\omega_c\tau$ as a function of fluence of implantation as follows.

Firstly, we plot the resonant linewidths as a function of applied magnetic field for each of the samples and observe that ΔH vs H can be represented by a straight line with a slope proportional to $1/\omega_c\tau$ (e.g., $\Delta H/H\sim1/\omega_c\tau$). Since the value of $\omega_c\tau$ for pristine HOPG at a magnetic field of $H=10$ T and helium temperature is on the order of 100, one can then estimate the decrease in $\omega_c\tau$ for the various implanted samples as the slope of ΔH vs H is increased.

Based on this analysis, the dependence of $\omega_c\tau$ on fluence ϕ was determined for the three ^{31}P-implanted samples studied in this work, and the results are given in Fig. 9. These results imply several interesting conclusions. Firstly, we can estimate the upper limit of fluence ϕ_{ul} that can be studied by the magnetoreflection experiment. For example, for the 70-keV ^{31}P-implanted sample ($T_i=600$ °C), we obtain $\phi_{ul}\sim5\times10^{15}$ cm^{-2}, based on a limiting value of $\omega_c\tau\sim5$.

These results also imply an estimate for the average implantation-induced degradation in the mean free path or carrier mobility. Based on this analysis, a degradation by a factor of 2.5 in $\omega_c\tau$ relative to unimplanted sample is obtained for a sample implanted at $T_i=600$ °C with 70-keV ^{31}P ions with a fluence $\phi=1\times10^{15}$ cm^{-2}. The magnetoreflection experiment, however, does not provide detailed information about the depth distribution of the mean free path, which would be necessary for the detailed interpretation of the transport measurements.

To obtain information on the change in carrier concentration due to ion implantation of graphite, infrared measurements in the vicinity of the allowed optical lattice mode at ~1580 cm^{-1} were carried out. Because the optical penetration depth is comparable to the ion-implantation depth, the infrared reflectivity is particularly sensitive to the implantation-induced change in carrier concentration. In contrast, transport measurements on bulk samples are relatively insensitive to implantation-induced changes because of the small ion penetration depth compared to typical sample dimensions.

Results for the implantation-induced change in the zero-field infrared reflectivity are shown in Fig. 3 for two

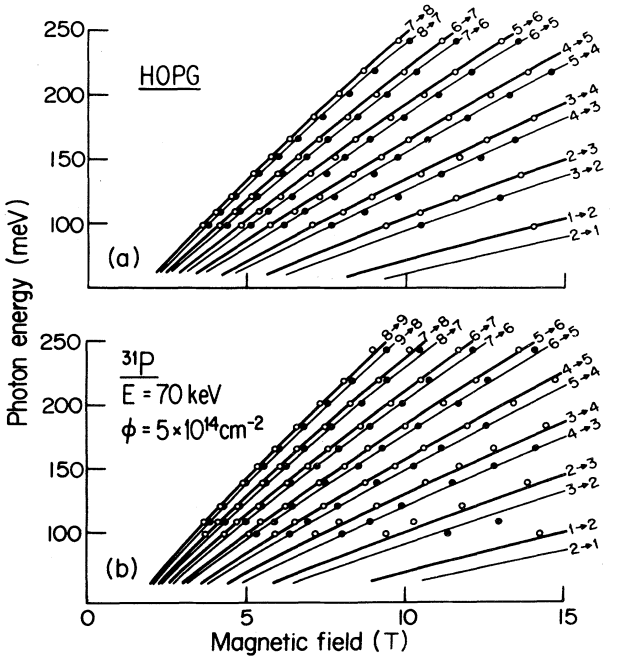

FIG. 8. Fan charts of the principal K-series transitions observed in the magnetoreflection experiment for the case of (a) pristine unimplanted HOPG and (b) HOPG ion-implanted with ^{31}P ($E=70$ keV) at $\phi=5\times10^{14}$ cm^{-2}. Data for both positive and negative polarizations are represented by closed and open circles, respectively. The points are experimental and the lines represent the least-squares fits to the points.

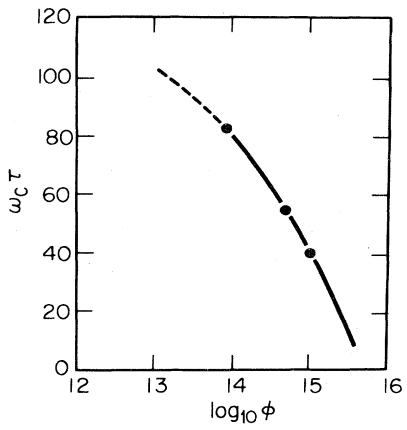

FIG. 9. Fluence dependence of the parameter $\omega_c\tau$. Notice that $\omega_c\tau\sim5$ corresponds to $\phi\sim5\times10^{15}$ cm^{-2}.

fluences of 70-keV ^{31}P-implanted HOPG in comparison with that for unimplanted HOPG. A previous line-shape analysis of the infrared spectra of graphite relates the line shape to the free-carrier contribution to the dielectric function.[27] For the case of pristine graphite, the room-temperature carrier concentration of 2×10^{19} cm^{-3} yields a line shape characterized by a reflectivity maximum. As the carrier concentration increases, the reflectivity maximum is transformed into a dispersion-type curve and finally at yet higher carrier concentrations a reflectivity minimum is obtained.[27] On the basis of the measured line shape for the 5×10^{14} cm^{-2} trace in Fig. 3, we estimate an average carrier concentration of 3×10^{20} cm^{-3} in the implanted region ($2\Delta R_p\sim440$ Å), which represents an increase in carrier concentration by a factor of ~15. The magnitudes of the increase in carrier density and decrease in carrier mobility are consistent with the implantation-induced change in resistivity reported by Endo *et al.* in ion-implanted graphite fibers.[29] It would be of interest to carry out resistivity measurements on highly ordered graphite fibers of ~10 μm diameter that are implanted under the same conditions as the samples used in the magnetoreflection experiment. Such measurements would permit a more meaningful comparison to be made between the implications of the magnetoreflection and zero-field infrared measurements on the actual transport measurements.

DISCUSSION

We should emphasize that the magnetoreflection experiment requires special conditions of implantation (e.g., hot-stage implantation at $T_i\gtrsim600$ °C) for several reasons. Firstly, hot-stage implantation preserves the crystallinity of the substrate, so that the condition $\omega_c\tau>1$ can be satisfied. It is important to mention that adequate crystallinity can be restored after room-temperature implantation only by subsequent annealing to temperatures very much higher than 600 °C.[4] However, at these higher annealing temperatures (above 2200 °C) a strong in-plane diffusion of foreign species takes place in graphite.[9] This means that during subsequent annealing at temperatures sufficiently high to gradually reduce the implantation-induced damage, most of the implanted ions would diffuse out of the substrate. This effect does not take place during hot-stage implantation, since it has been demonstrated[30] that the concentration and spatial distribution of ions implanted into graphite are nearly the same after hot-stage implantation as after room-temperature implantation. This implies that the effect of implantation is manifested not only through implantation-induced defects but also through long-range strain effects due to the implanted ions resident in the samples.

It should be noted that the magnitude and sign of the shifts observed in γ_0 and γ_1 are in agreement with the expected consequences of a long-range strain induced by implantation. The strong in-plane coupling in graphite implies that only a very small in-plane expansion, and therefore a very small decrease in γ_0, is expected. Most of the excess volume introduced by the implanted ions should be accommodated by expansion along the c axis, leading to a decrease in the interplanar coupling and therefore in γ_1. However, even in pristine graphite the interplanar coupling is very weak, and so a large expansion along the c axis leads to only a small ($\sim15\%$) change in γ_1, as is observed.

To prevent fracture of the bulk sample, an in-plane lattice expansion must also occur in the regions of the sample containing no implanted ions. Since the magnetoreflection spectra exhibit relatively small line broadening compared with the unimplanted graphite samples, we infer that the variation of $\Delta a_0/a_0$ along the c axis is long range. Thus, if we write $\Delta a_0/a_0\sim e^{-d/\xi}$, where d is measured relative to R_p along the c axis and the coherence length ξ is very large compared with the c-axis lattice constant ($\xi\gg c_0$), the magnetoreflection results imply that ξ is also larger than the optical skin depth, δ.

Relaxation of the in-plane lattice expansion $\Delta a_0/a_0\sim\exp(-d/\xi)$ as we move away from R_p causes carbon atoms in adjacent layers to be slightly displaced from their normal equilibrium positions on a potential-energy diagram. Because of the hard-core potential at small distances, such a displacement from equilibrium favors a lattice expansion and hence a decrease in γ_1, in agreement with observations. The relaxation of this lattice expansion occurs via lattice dislocations and ξ is proportional to the dislocation density.

According to our model, the magnetoreflection signal is dominated by contributions from regions (1) and (3) in Fig. 10, and the present results show that these two regions contribute coherently to the magnetoreflection signal with essentially the same values of γ_0 and γ_1 throughout the optical skin depth. When an ion beam with high energy and velocity enters the sample, the energy loss is primarily from electron plasma excitations and lattice damage per unit length is small initially [region (1)], so we expect little decrease of $\omega_c\tau$ in this region. As the ion velocity is reduced, the lattice damage is increased, so that a major reduction in $\omega_c\tau$ can be expected. Because

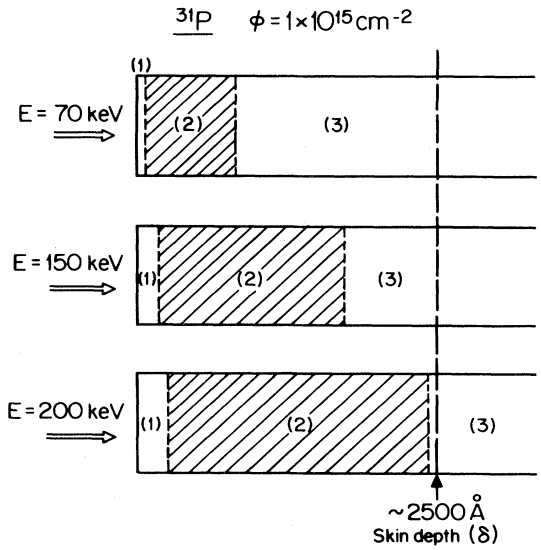

FIG. 10. Schematic view of the spatial distribution of the damage produced in the substrate for different energies of implantation (see text).

of the large lattice distortion in the region where the ions come to rest, here too $\omega_c\tau$ is expected to be significantly decreased. We thus refer to region (2) in Fig. 10 as the region of significant lattice damage and reduced $\omega_c\tau$. The spatial extent of region (2) can be determined by Rutherford backscattering.[31] Beyond region (2), the graphite sees little damage, the condition $\omega_c\tau \gg 1$ is again obeyed, and coherent contributions to the magnetoreflection spectrum from regions (1) and (3) can take place. Being near the surface, region (1) has the highest optical energy density; however, region (1) has a smaller τ than region (3). Thus, referring to Fig. 10, we see that the lower the energy of implantation, the smaller the fraction of the optical penetration depth that has significant ion-induced lattice damage.

To relate these arguments to the magnetoreflection experiment we now present explicit spectra from ^{31}P-ion-implanted HOPG as a function of the energy of implantation. For a sample implanted with ^{31}P ions at a fluence of 1×10^{15} cm^{-2} and an implantation energy of 150 keV the penetration depth is $R_p \sim 1480$ Å and $\Delta R_p \sim 390$ Å. Under these conditions, some Landau-level transitions were observable for photon energies of $\hbar\omega < 140$ meV or less, but the resonances were of low intensity and were quite broad. The uncertainty in the determination of m^* for this sample was therefore very large due both to the uncertainty in the resonant fields and to the small number of transitions available for the least-squares fit. The resulting uncertainty in m^* was larger than its deviation from the value for HOPG. We also note that for a graphite sample implanted with ^{31}P ions at 200 keV with a fluence of 1×10^{15} cm^{-2}, both the H- and K-point oscillations were reduced to the noise level of the measurements.

As noted above, the observed behavior of the spectra as a function of the energy of implantation can be understood upon closer examination of the spatial distribution of the damage to the substrate during hot-stage implantation.[31] In making this argument, we note that only the volume within the optical skin depth δ contributes to the magnetoreflection spectra (see Fig. 10). Thus as the ion energy increases, there results a decrease in the sample volume within the optical skin depth for which $\omega_c\tau \gg 1$. This argument explains why the signal from the 150-keV ^{31}P-implanted sample is strongly attenuated and from the 200-keV ^{31}P-implanted sample is washed out completely.

The attenuation of the magnetoreflection resonances with increasing photon energy is also of significance. For example, it is observed that the resonances in the magnetoreflection spectra from the 150-keV ^{31}P-implanted sample are gradually attenuated as $\hbar\omega$ increases to 140 meV. This effect is attributed to the frequency dependence of the optical skin depth. Specifically, as $\hbar\omega$ increases, δ is decreased so that the most crystalline portion of the sample [region (3) on Fig. 10] does not contribute significantly to the spectra at higher photon energies.

The band overlap in graphite is almost completely determined by the SWMcC band parameter γ_2. Since γ_2 depends on interplanar interactions two layers apart, and γ_1 depends on interplanar interactions between atoms on adjacent layers, we can expect $\Delta\gamma_2/\gamma_2 \approx 2\Delta\gamma_1/\gamma_1$, as has been previously noted by several authors.[32–34] The observed implantation-induced decrease in γ_1 would thus imply a decrease in the band overlap and consequently also in carrier density. The infrared reflectivity measurements (Fig. 3), however, imply an increase in carrier density, suggesting that implantation moves the Fermi level, creating an imbalance between the electron and hole concentrations.

Since the decrease in γ_2 is expected to occur only over the correlation length ξ, transport measurements in graphite fibers should provide information on ξ. According to the model in Fig. 10, implantation of a graphite fiber should give rise to a circuit composed of parallel resistors along the fiber length: The region modified by implantation with coherence length ξ will have a higher carrier density, but a lower relaxation time as compared to the remaining region, which is modeled by the parameters of the unimplanted graphite fiber. If the effective enhancement in carrier density is greater than the effective decrease of the relaxation time, the fiber will show an increase in conductivity. Preliminary results by Endo *et al.*[29] indicate a 5% decrease in conductivity for fibers implanted with ^{11}B ions at 100 keV to a fluence of 2.8×10^{15} ions/cm^{-2}. It would be of interest to examine the conductivity of fibers implanted under the same conditions as the magnetoreflection experiment, though the changes in conductivity for such fibers might be too small to measure conveniently.

ACKNOWLEDGMENTS

We wish to thank Mr. M. Rothman and M. Hom for assistance with the ion implantation, Mr. F. Paine for help during construction of the hot-stage sample holder, Dr. A. W. Moore of the Union Carbide Corporation for the generous donation of the HOPG material, and Professor J. W. McClure for numerous helpful discussions. The experimental work was carried out at the Francis Bitter National Magnet Laboratory (FBNML). We acknowledge L. Rubin and B. Brandt of the FBNML for technical assistance. We also gratefully acknowledge U.S. Navy Office of Naval Research Grant No. N00014-77-C-0053 for support. The FBNML is supported by the National Science Foundation.

*Present address: Department of Physics, Boston University, Boston, MA 02215.

†Present address: IBM Research Center, P.O. Box 218, Yorktown Heights, N.Y. 10598.

[1] J. W. Mayer, L. Eriksson, and J. A. Davis, *Ion Implantation in Semiconductors* (Academic, New York, 1970).

[2] J. E. Smith, Jr., M. H. Brodsky, B. L. Crowder, and M. I. Nathan, J. Non-Cryst. Solids 8-10, 179 (1972).

[3] B. S. Elman, M. S. Dresselhaus, G. Dresselhaus, E. W. Maby, and H. Mazurek, Phys. Rev. B 24, 1027 (1981).

[4] B. S. Elman, M. Shayegan, M. S. Dresselhaus, H. Mazurek, G. Dresselhaus, Phys. Rev. B 25, 4142 (1982); M. Shayegan, B. S.

Elman, H. Mazurek, M. S. Dresselhaus, and G. Dresselhaus, in *Metastable Materials Formation by Ion Implantation,* edited by S. T. Picraux and W. J. Choyke (North-Holland, New York, 1982), p. 417.

[5]B. S. Elman, M. Hom, E. W. Maby, and M. S. Dresselhaus, in *Intercalated Graphite,* edited by M. S. Dresselhaus, G. Dresselhaus, J. E. Fisher, and M. J. Moran (North-Holland, New York, 1983), p. 341.

[6]C. Nicolini, T. C. Chieu, G. Dresselhaus, and M. S. Dresselhaus, Solid State Commun. 43, 233 (1982).

[7]W.-K. Chu, J. W. Mayer, and M.-A. Nicolet, *Backscattering Spectrometry* (Academic, New York, 1978).

[8]L. C. Feldman, J. W. Mayer, and S. T. Picraux, *Materials Analysis by Ion Channeling* (Academic, New York, 1982).

[9]T. Venkatesan, B. S. Elman, G. Braunstein, M. S. Dresselhaus, and G. Dresselhaus (unpublished).

[10]B. Lax and J. G. Mavroides, in *Solid State Physics,* edited by F. Seitz and D. Turnbull (Academic, New York, 1960), Vol. 11.

[11]M. H. Weiler, in *Semiconductors and Semimetals,* edited by R. K. Willardson and A. C. Beer (Academic, New York, 1981); M. H. Weiler, Ph.D. thesis, Massachusetts Institute of Technology, 1977 (unpublished).

[12]M. S. Dresselhaus, in *Proceedings of the International Conference on Semimetals and Narrow Gap Semiconductors,* edited by D. L. Carter and R. T. Bate (Pergamon, New York, 1971), p. 3.

[13]R. N. Brown, J. G. Mavroides, and B. Lax, Phys. Rev. 129, 2055 (1963).

[14]M. S. Maltz and M. S. Dresselhaus, Phys. Rev. B 2, 2877 (1970).

[15]P. R. Schroeder, M. S. Dresselhaus, and A. Javan, in *Proceedings of the International Conference on Semimetals and Narrow Gap Semiconductors,* edited by D. L. Carter and R. T. Bate (Pergamon, New York, 1971), p. 139.

[16]P. R. Schroeder, Ph.D. thesis, Massachusetts Institute of Technology, 1969 (unpublished).

[17]W. W. Tov, M. S. Dresselhaus, and G. Dresselhaus, Phys. Rev. B 15, 4077 (1977).

[18]E. Mendez, A. Misu, and M. S. Dresselhaus, Phys. Rev. B 21, 827 (1980).

[19]M. P. Vecchi and M. S. Dresselhaus, Phys. Rev. B 10, 771 (1974).

[20]E. Mendez, T. C. Chieu, N. Kambe, and M. S. Dresselhaus, Solid State Commun. 33, 837 (1980).

[21]E. Kunoff, B. S. Elman, and M. S. Dresselhaus (unpublished).

[22]J. C. Slonczewski and P. R. Weiss, Phys. Rev. 109, 272 (1958).

[23]J. W. McClure, Phys. Rev. 108, 612 (1957); 119, 606 (1960).

[24]A. W. Moore, in *Chemistry and Physics of Carbon,* edited by P. L. Walker and P. A. Thrower (Dekker, New York, 1973), Vol. 11, p. 69.

[25]Calculated from the Lindhard-Scharff-Schiott theory [J. Lindhard, M. Scharff, and H. E. Schiott, K. Dan. Vidensk. Selsk. Mat. Fys. Medd. 33, 14 (1963)] and electronic stopping-power tables [L. C. Northcliffe and R. F. Schilling, Nucl. Sect. A 7, 233 (1970)].

[26]F. Tuinstra and J. L. Koenig, J. Chem. Phys. 53, 1126 (1970).

[27]S. Y. Leung, Ph.D. thesis, Massachusetts Institute of Technology, 1980 (unpublished).

[28]A. Misu, E. Mendez, and M. S. Dresselhaus, J. Phys. Soc. Jpn. 47, 199 (1979).

[29]M. Endo, T. C. Chieu, G. Timp, M. S. Dresselhaus, and B. S. Elman, Phys. Rev. B 28, 6982 (1983).

[30]G. Braunstein, B. S. Elman, M. S. Dresselhaus, G. Dresselhaus, and T. Venkatesan (unpublished).

[31]L. McNeil, B. S. Elman, M. S. Dresselhaus, G. Dresselhaus, and T. Venkatesan (unpublished).

[32]K. Noto and T. Tsuzuku, Carbon 12, 349 (1974).

[33]I. L. Spain, Carbon 14, 229 (1976).

[34]H. Nagayoshi, J. Phys. Soc. Jpn. 43, 760 (1977).